

A Simple and Fast Iterative Soft-thresholding Algorithm for Tight Frames in Compressed Sensing Magnetic Resonance Imaging

Yunsong Liu, Zhifang Zhan, Jian-Feng Cai, Di Guo, Zhong Chen, Xiaobo Qu*

Abstract—Compressed sensing has shown great potentials in accelerating magnetic resonance imaging. Fast image reconstruction and high image quality are two main issues faced by this new technology. It has been shown that, redundant image representations, e.g. tight frames, can significantly improve the image quality. But how to efficiently solve the reconstruction problem with these redundant representation systems is still challenging. This paper attempts to address the problem of applying fast iterative soft-thresholding algorithm (FISTA) to tight frames based magnetic resonance image reconstruction. By introducing the canonical dual frame, we construct an orthogonal projection operator on the range of the analysis sparsity operator and propose a new algorithm, called the projected FISTA (pFISTA). We theoretically prove that pFISTA converges to the minimum of a function with a balanced tight frame sparsity. One major advantage of pFISTA is that only one extra parameter, the step size, is introduced and the numerical solution is stable to it in terms of image reconstruction errors, thus allowing easily setting in many fast magnetic resonance imaging applications.

Index Terms—Sparse Models, Iterative Thresholding, Tight Frames, Compressed Sensing, MRI

I. INTRODUCTION

MAGNETIC resonance imaging (MRI) plays an important role in clinical diagnosis nowadays. MRI is noninvasive and can provide high quality images, especially for soft tissues. One major challenge that MRI faces is the fundamental limitation of its imaging speed both physically, e.g. gradient amplitude and slew-rate, and physiologically, e.g. nerve stimulation, [1]. Compressed sensing (CS) [1-3] is a promising

technique to accelerate MRI by undersampling its signals, k-space data or better known as Fourier space data. This new technology is called compressed sensing MRI [1], or CS-MRI for short. The undersampling process can be mathematically modeled as

$$\mathbf{y} = \mathbf{U}\mathbf{F}\mathbf{x} + \boldsymbol{\eta} \quad (1.1)$$

where $\mathbf{x} \in \mathbb{C}^N$ represents the magnetic resonance (MR) image that is rearranged to be a column vector, $\mathbf{F} \in \mathbb{C}^{N \times N}$ is the discrete Fourier transform, $\mathbf{U} \in \mathbb{R}^{M \times N}$ ($M < N$) is the undersampling matrix, $\boldsymbol{\eta} \in \mathbb{C}^M$ is the additive noise, and $\mathbf{y} \in \mathbb{C}^M$ is the undersampled k-space data. The goal of image reconstruction is to recover a reasonable \mathbf{x} with N pixels from \mathbf{y} with M data points, and thus it is an ill-posed problem. CS-MRI solves this problem by introducing the sparsity assumptions on MRI images in certain transform domains such as total variation and wavelet domain [1]. Mathematically, sparsity is promoted directly by the ℓ_0 norm. However, the ℓ_0 norm based CS problems are NP-hard and thus are intractable [3]. The ℓ_1 norm is a good relaxation that can work as well as ℓ_0 norm under some conditions, and more practically the reconstruction problem can be solved efficiently with convex optimization methods [2, 3].

Equipped with the ℓ_1 norm to enforce sparsity, one still has to decide how to model the CS-MRI problem. Commonly, there are two kinds of models that are synthesis models and analysis models [4-6]:

$$\text{Synthesis: } \min_{\mathbf{a}} \lambda \|\mathbf{a}\|_1 + \frac{1}{2} \|\mathbf{y} - \mathbf{U}\mathbf{F}\boldsymbol{\Phi}\mathbf{a}\|_2^2 \quad (1.2)$$

$$\text{Analysis: } \min_{\mathbf{x}} \lambda \|\boldsymbol{\Psi}\mathbf{x}\|_1 + \frac{1}{2} \|\mathbf{y} - \mathbf{U}\mathbf{F}\mathbf{x}\|_2^2, \quad (1.3)$$

where $\boldsymbol{\Psi}$ is an analysis operator, $\boldsymbol{\Phi}$ is a synthesis operator, and \mathbf{a} is the coefficient that is synthesized by $\boldsymbol{\Phi}$ to be an image, meaning that $\mathbf{x} = \boldsymbol{\Phi}\mathbf{a}$. λ is called the regularization parameter that is related to noise level and λ is chosen as a trade-off between sparsity and data fidelity. For an orthonormal basis with $\boldsymbol{\Psi}$ and $\boldsymbol{\Phi} = \boldsymbol{\Psi}^* = \boldsymbol{\Psi}^{-1}$ ($\boldsymbol{\Psi}^*$ and $\boldsymbol{\Psi}^{-1}$ denote the conjugate transpose and the inverse of $\boldsymbol{\Psi}$, respectively) its analysis and synthesis operators respectively, the analysis model and synthesis model yield the same solutions [6]. The

This work was supported by the NNSF of China (61201045, 61302174 and 11375147), Natural Science Foundation of Fujian Province, China (2015J01346), Fundamental Research Funds for the Central Universities (2013SH002) and Scientific Research Foundation for the Introduction of Talent at Xiamen University of Technology (YKJ12021R) and NSF DMS-1418737. (*Corresponding author: Xiaobo Qu)

Yunsong Liu, Zhifang Zhan, Zhong Chen and Xiaobo Qu are with the Department of Electronic Science, Fujian Provincial Key Laboratory of Plasma and Magnetic Resonance, Xiamen University, Xiamen, China (e-mail: yunsongliu@stu.xmu.edu.cn; zhanzfadu@stu.xmu.edu.cn; chenz@xmu.edu.cn; quxiaobo@xmu.edu.cn)

Jian-Feng Cai is with the Department of Mathematics, University of Iowa, Iowa City, USA (e-mail: jianfeng-cai@uiowa.edu)

Di Guo is with the School of Computer and Information Engineering, Fujian Provincial University Key Laboratory of Internet of Things Application Technology, Xiamen University of Technology, Xiamen, China (e-mail: guodi@xmut.edu.cn)

redundant system, such as a frame and a dictionary, can benefit from that redundancy in noise removal and artifacts reduction in signal processing [5, 7, 8]. Within the field of CS-MRI, the quality of reconstructed images is improved with redundant systems [9-13]. For these redundant systems, these two models are totally different [6, 10, 14, 15]. Theoretically, CS theory [5] reveals that analysis models works under a wider range of dictionaries than synthesis models, and it was proved in [16] that analysis models converge to some partial differential equation models with geometric interpretations. In practice, researchers in signal processing observed that analysis models reaches lower reconstructed error than synthesis models and are their suggestions for signal processing [6, 10, 14, 15].

Iterative soft-thresholding algorithm (ISTA) is a kind of simple and efficient algorithm for the ℓ_1 -norm based sparse recovery problems [17-22]. An accelerated version of ISTA termed as fast iterative shrinkage-thresholding algorithm (FISTA) [23] was proposed to utilize the previous two iterations in a special way to further speed up the convergence of ISTA. The efficiencies of both ISTA and FISTA depend on the simplicity of computing the proximal map of the non-smooth ℓ_1 norm based functions in objectives. The proximal map of a function f is defined as [19, 24]

$$\text{prox}_f(\mathbf{x}) = \arg \min_{\mathbf{z}} f(\mathbf{z}) + \frac{1}{2} \|\mathbf{z} - \mathbf{x}\|_2^2. \quad (1.4)$$

For a synthesis model as (1.2), $f(\boldsymbol{\alpha}) = \lambda \|\boldsymbol{\alpha}\|_1$, the proximal map is

$$\text{prox}_f(\boldsymbol{\alpha}) = \arg \min_{\mathbf{z}} \lambda \|\mathbf{z}\|_1 + \frac{1}{2} \|\mathbf{z} - \boldsymbol{\alpha}\|_2^2 = T_\lambda(\boldsymbol{\alpha}). \quad (1.5)$$

where $T_\lambda(\cdot)$ is a point wise soft-thresholding function defined as

$$T_\lambda(\alpha_i) = \max\{|\alpha_i| - \lambda, 0\} \cdot \frac{\alpha_i}{|\alpha_i|}. \quad (1.6)$$

The simplicity of the proximal map (1.5) makes FISTA very efficient for synthesis models. Whereas for analysis models, there is no such simple closed form solution for the proximal map of $f(\mathbf{x}) = \lambda \|\Psi\mathbf{x}\|_1$, resulting in challenges to apply FISTA to solve analysis models.

To address this problem, Tan., *et al.* [25] proposed two methods, namely, smoothing FISTA (SFISTA) and decomposition FISTA. They argue that SFISTA converges faster than decomposition FISTA in both theory and numerical experiments for tight frames [25]. SFISTA replaces the non-smooth term $f(\mathbf{x}) = \lambda \|\Psi\mathbf{x}\|_1$ by its Moreau envelop defined as [25]

$$f_\mu(\mathbf{x}) = \min_{\mathbf{z}} \lambda \|\Psi\mathbf{z}\|_1 + \frac{1}{2\mu} \|\mathbf{z} - \mathbf{x}\|_2^2, \quad (1.7)$$

which is smooth. Then, they apply FISTA to solve this relaxed smooth optimization problem. As it is shown in [25] and our numerical experiments, both the convergence speed and reconstructed error of SFISTA are sensitive to the smooth approximate parameter μ . By introducing the continuation strategy to gradually decreasing the value of μ , Tan., *et al.*

argue that the solution of the previous problem with larger μ will provide a warm start of the current problem with smaller μ and thus can make SFISTA converge fast with high accuracy of the smooth approximation [25]. Despite the effectiveness of this continuation strategy which they verified in numerical experiments [25], it introduces more parameters, such as the decrease rate, the maximum number of iterations for a sub-problem with a specific value of μ , which makes SFISTA complicated for CS-MRI applications.

In this paper, we will address the problem to apply FISTA to analysis models for tight frames in CS-MRI. For a general frame, the synthesis operator is often chosen as its canonical dual frame defined as [26]

$$\Phi = (\Psi^* \Psi)^{-1} \Psi^*, \quad (1.8)$$

which is also known as the pseudo-inverse of Ψ [6]. (1.8) directly leads to the property

$$\Phi \Psi = \mathbf{I}. \quad (1.9)$$

Another nice property of (1.8) is that the operator

$$P = \Psi \Phi \quad (1.10)$$

is the orthogonal projection [26] on $\text{Range}(\Psi) = \{\Psi\mathbf{x} \mid \mathbf{x} \in \mathbb{C}^N\}$ as illustrated in Fig. 1.

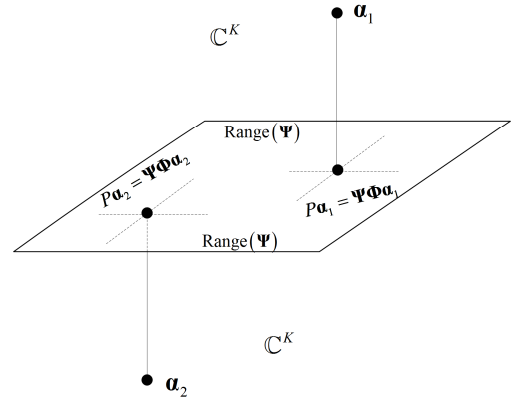


Fig. 1. Illustration of the orthogonal projection operation on $\text{Range}(\Psi)$.

As an orthogonal projection, the operator P has

$$P\boldsymbol{\alpha} = \Psi\Phi\boldsymbol{\alpha} = \boldsymbol{\alpha}, \quad (1.11)$$

for $\boldsymbol{\alpha} \in \text{Range}(\Psi)$. By introducing the canonical dual frame, we obtain an equivalent synthesis-like model of (1.3). Then we apply FISTA to this equivalent model. In order to keep the simplicity of FISTA, we replace a constrained proximal map by an unconstrained proximal map plus the orthogonal projection in (1.10). Therefore, the proposed algorithm is called projected FISTA (pFISTA). We will prove that pFISTA converges to the following model

$$\min_{\boldsymbol{\alpha}} \lambda \|\boldsymbol{\alpha}\|_1 + \frac{1}{2} \|\mathbf{y} - \mathbf{U}\Phi\boldsymbol{\alpha}\|_2^2 + \frac{1}{2\gamma} \|(\mathbf{I} - \Psi\Phi)\boldsymbol{\alpha}\|_2^2 \quad (1.12)$$

with $0 < \gamma \leq 1$ is the step size. Model (1.12) is an approximation of the analysis model (1.14) and gives reconstructed images similar to the analysis model. When Ψ is tight, (1.12) is the balanced model in [10, 27, 28]. In numerical experiments, we will verify the efficiency of pFISTA by comparing it with

FISTA and the state-of-the-art SFISTA.

II. PROPOSED METHOD

In this section, we first rewrite the analysis model as an equivalent constrained synthesis-like one and then propose the pFISTA to solve the tight-frames-based CS-MRI problems.

A. Projected Fast Iterative Soft-Thresholding Algorithm

With the choice of Φ as the canonical dual frame of Ψ , the analysis model in (1.3) is equivalent to the following form

$$\min_{\alpha \in \text{Range}(\Psi)} \lambda \|\alpha\|_1 + \frac{1}{2} \|\mathbf{y} - \mathbf{U}\mathbf{F}\Phi\alpha\|_2^2. \quad (1.16)$$

The equivalence means that the solutions of (1.3) and (1.16) are the same. The proof of this equivalence is in the Appendix.

To handle the constraint in the synthesis-like analysis model in (1.16), we introduce an indicator function

$$d(\alpha) = \begin{cases} 0 & , \alpha \in \text{Range}(\Psi) \\ \infty & , \alpha \notin \text{Range}(\Psi) \end{cases} \quad (1.17)$$

to obtain an equivalent unconstrained model of (1.16) as

$$\min_{\alpha} \lambda \|\alpha\|_1 + \frac{1}{2} \|\mathbf{y} - \mathbf{U}\mathbf{F}\Phi\alpha\|_2^2 + d(\alpha). \quad (1.18)$$

We further denote

$$\begin{aligned} g(\alpha) &= \lambda \|\alpha\|_1 + d(\alpha) \\ f(\alpha) &= \frac{1}{2} \|\mathbf{y} - \mathbf{U}\mathbf{F}\Phi\alpha\|_2^2 \end{aligned} \quad (1.19)$$

where $g(\alpha)$ is a non-smooth convex function, and $f(\alpha)$ is a smooth function with a Lipschitz continuous gradient and the Lipschitz constant $L_f = \|\Phi^* \mathbf{F}^* \mathbf{U}^T \mathbf{U}\mathbf{F}\Phi\|_2$. Then, we apply FISTA [23] to solve the model in (1.18) by incorporating the proximal mapping

$$\begin{aligned} \alpha_{k+1} &= \text{prox}_{\gamma g}(\alpha_k - \gamma \nabla f(\alpha_k)) \\ &= \arg \min_{\alpha} \lambda \gamma \|\alpha\|_1 + \frac{1}{2} \left\| \alpha - (\alpha_k - \gamma \nabla f(\alpha_k)) \right\|_2^2 + d(\alpha), \quad (1.20) \\ &= \arg \min_{\alpha \in \text{Range}(\Psi)} \lambda \gamma \|\alpha\|_1 + \frac{1}{2} \left\| \alpha - (\alpha_k - \gamma \nabla f(\alpha_k)) \right\|_2^2 \end{aligned}$$

where γ is the step size.

So far, we have converted the original analysis-based CS-MRI problem into a much simpler form in (1.20) where the objective function is separable. However, the appearance of the constraint makes it hard to find an analytical solution of (1.20). Observing that without the constraint, the closed form solution of (1.20) is

$$\tilde{\alpha}_{k+1} = T_{\gamma\lambda} \left((\alpha_k - \gamma \nabla f(\alpha_k)) \right), \quad (1.21)$$

we propose to replace (1.20) by

$$\begin{aligned} \tilde{\alpha}_{k+1} &= T_{\gamma\lambda} \left((\alpha_k - \gamma \nabla f(\alpha_k)) \right), \\ \alpha_{k+1} &= P_{\text{Range}(\Psi)}(\tilde{\alpha}_{k+1}) \end{aligned} \quad (1.22)$$

where $P_{\text{Range}(\Psi)}$ is the orthogonal projection operator on the $\text{Range}(\Psi)$. More specifically, for our problem in (1.16), this replacement leads to

$$\tilde{\alpha}_{k+1} = T_{\gamma\lambda} \left((\alpha_k + \gamma \Psi(\Psi^* \Psi)^{-1} \mathbf{F}^* \mathbf{U}^T (\mathbf{y} - \mathbf{U}\mathbf{F}\Phi\alpha_k)) \right). \quad (1.23)$$

$$\alpha_{k+1} = \Psi\Phi\tilde{\alpha}_{k+1}$$

The two steps in (1.23) can be incorporated to be

$$\alpha_{k+1} = T_{\gamma\lambda} \left(\Psi \left(\Phi\alpha_k + \gamma (\Psi^* \Psi)^{-1} \mathbf{F}^* \mathbf{U}^T (\mathbf{y} - \mathbf{U}\mathbf{F}\Phi\alpha_k) \right) \right). \quad (1.24)$$

Furthermore, by substituting the coefficients α by images $\mathbf{x} = \Phi\alpha$, we get that

$$\mathbf{x}_{k+1} = \Phi T_{\gamma\lambda} \left(\Psi \left(\mathbf{x}_k + \gamma (\Psi^* \Psi)^{-1} \mathbf{F}^* \mathbf{U}^T (\mathbf{y} - \mathbf{U}\mathbf{F}\mathbf{x}_k) \right) \right). \quad (1.25)$$

For a tight frame, we have $\Phi = \Psi^*$ and (1.25) becomes

$$\mathbf{x}_{k+1} = \Psi^* T_{\gamma\lambda} \left(\Psi \left(\mathbf{x}_k + \gamma \mathbf{F}^* \mathbf{U}^T (\mathbf{y} - \mathbf{U}\mathbf{F}\mathbf{x}_k) \right) \right) \quad (1.26)$$

All the above derivations lead to the proposed projected fast iterative soft-thresholding algorithm (pFISTA) for tight frames in CS-MRI. This algorithm is summarized in Algorithm 1.

Algorithm 1: pFISTA for tight frames in CS-MRI

Parameters: λ, γ

Initialization: $t_0 = 1, \mathbf{x}_0, \hat{\mathbf{x}}_0$

While not converge, do

$$\mathbf{x}_{k+1} = \Psi^* T_{\gamma\lambda} \left(\Psi \left(\hat{\mathbf{x}}_k + \gamma \mathbf{F}^* \mathbf{U}^T (\mathbf{y} - \mathbf{U}\mathbf{F}\hat{\mathbf{x}}_k) \right) \right)$$

$$t_{k+1} = \frac{1 + \sqrt{1 + 4t_k^2}}{2}$$

$$\hat{\mathbf{x}}_{k+1} = \mathbf{x}_{k+1} + \frac{t_k - 1}{t_{k+1}} (\mathbf{x}_{k+1} - \mathbf{x}_k)$$

Output: \mathbf{x}_{n+1}

The pFISTA owns the following advantages:

1) Low Memory Consumption

The proposed pFISTA operates on images instead of transform, e.g. wavelet, coefficients in the original FISTA. Furthermore, pFISTA does not require any auxiliary frame coefficients used in popular analysis model solvers of such as ADMM [29-31] (a.k.a. split Bregman [28] for tight frames). These can significantly reduce the memory consumption since coefficients need more memory than images for a redundant frame system. For example, in our numerical experiment, the number of redundant wavelet coefficients for an image is 13 times as many as the number of image pixels. Thus, the pFISTA is memory saving for large scale data and highly redundant representation systems.

2) Simplicity

The simplicity of pFISTA means that besides the regularization parameter, there is only one free parameter, the step size γ , needs to be set. Besides, it will be shown that this parameter only affects the convergence speed but not change the empirical image reconstruction errors although different tight frames are used to represent MRI images. Thus, we recommend users to set $\gamma = 1$ for low reconstruction error and fast convergence speed.

3) Fast Computation and Superior Image Quality

Fast computation means that pFISTA inherits fast convergence of FISTA as it will be shown in experiments. Moreover, since pFISTA is an approximate solver for analysis models, it gives images with better quality than FISTA for synthesis models.

B. Convergence Analysis

Theorem 1: Let $\{\mathbf{x}_k\}$ be generated by **Algorithm 1**, then the sequence $\{\mathbf{a}_k\} = \{\Psi\mathbf{x}_k\}$ converges to the solution of

$$\min_{\mathbf{a}} \lambda \|\mathbf{a}\|_1 + \frac{1}{2} \|\mathbf{y} - \mathbf{U}\mathbf{F}\Psi^* \mathbf{a}\|_2^2 + \frac{1}{2\gamma} \|(\mathbf{I} - \Psi\Psi^*) \mathbf{a}\|_2^2 \quad (1.27)$$

provided that the step size $0 < \gamma \leq 1$ and Ψ is a tight frame.

And $\{\mathbf{a}_k\}$ satisfies

$$F(\mathbf{a}_k) - F(\mathbf{a}^*) \leq \frac{2 \|\mathbf{a}_0 - \mathbf{a}^*\|_2^2}{\gamma(k+1)^2} \quad (1.28)$$

where \mathbf{a}^* is an arbitrary solution of (1.27) and $F(\cdot)$ is the objective function in (1.27).

Proof of Theorem 1:

Let us denote

$$\begin{aligned} h(\mathbf{a}) &= \lambda \|\mathbf{a}\|_1 \\ u(\mathbf{a}) &= \frac{1}{2} \|\mathbf{y} - \mathbf{U}\mathbf{F}\Psi^* \mathbf{a}\|_2^2 + \frac{1}{2\gamma} \|(\mathbf{I} - \Psi\Psi^*) \mathbf{a}\|_2^2. \end{aligned} \quad (1.29)$$

Then applying FISTA [23] to (1.27) with step size γ results in the iterations

$$\begin{aligned} \mathbf{a}_{k+1} &= \text{prox}_{\gamma h}(\mathbf{a}_k - \gamma \nabla u(\mathbf{a}_k)) \\ &= T_{\gamma \lambda}(\Psi(\Psi^* \mathbf{a}_k + \gamma \mathbf{F}^* \mathbf{U}^T (\mathbf{y} - \mathbf{U}\mathbf{F}\Psi^* \mathbf{a}_k))) \end{aligned} \quad (1.30)$$

Multiplying both sides by Ψ^* and letting $\mathbf{x}_k = \Psi^* \mathbf{a}_k$, we get

$$\mathbf{x}_{k+1} = \Psi^* T_{\gamma \lambda}(\Psi(\mathbf{x}_k + \gamma \mathbf{F}^* \mathbf{U}^T (\mathbf{y} - \mathbf{U}\mathbf{F}\mathbf{x}_k))). \quad (1.31)$$

This is exactly the same procedure of pFISTA in **Algorithm 1**.

The next question is that can we insure the convergence? By definition, the Lipschitz constant for the gradient of ∇u is

$$L(\gamma) = L(\nabla u) = \left\| \Psi\mathbf{F}^* \mathbf{U}^T \mathbf{U}\mathbf{F}\Psi^* + \frac{1}{\gamma} (\mathbf{I} - \Psi\Psi^*) \right\|_2. \quad (1.32)$$

According to [23], if the step size satisfies

$$\gamma \leq 1/L(\gamma), \quad (1.33)$$

or equivalently

$$L(\gamma) \leq 1/\gamma, \quad (1.34)$$

then (1.31) will converge.

We will prove that

$$\begin{cases} L(\gamma) = 1/\gamma, & 0 < \gamma \leq 1 \\ L(\gamma) \leq 1, & \gamma > 1 \end{cases}. \quad (1.35)$$

Proof of (1.35):

For simplicity, we denote

$$\mathbf{B} = \Psi\mathbf{F}^* \mathbf{U}^T \mathbf{U}\mathbf{F}\Psi^* - \frac{1}{\gamma} \Psi\Psi^* = \Psi\mathbf{F}^* \left(\mathbf{U}^T \mathbf{U} - \frac{1}{\gamma} \mathbf{I} \right) \mathbf{F}\Psi^*, \quad (1.36)$$

then we have

$$L(\gamma) = \left\| \mathbf{B} + \frac{1}{\gamma} \mathbf{I} \right\|_2 = \max_i \left\{ \lambda_i(\mathbf{B}) + \frac{1}{\gamma} \right\} \quad (1.37)$$

where $\lambda_i(\mathbf{B})$ means the i^{th} eigenvalue of \mathbf{B} because $\mathbf{B} + 1/\gamma \mathbf{I}$ is a Hermitian matrix. Therefore, we need to analyze $\lambda_i(\mathbf{B})$. We have

$$\begin{aligned} \Psi\mathbf{F}^* \left(\mathbf{U}^T \mathbf{U} - \frac{1}{\gamma} \mathbf{I} \right) \mathbf{F}\Psi^* \mathbf{a} &= \lambda \mathbf{a} \\ \Rightarrow \left(\mathbf{U}^T \mathbf{U} - \frac{1}{\gamma} \mathbf{I} \right) \mathbf{F}\Psi^* \mathbf{a} &= \lambda \mathbf{F}\Psi^* \mathbf{a} \end{aligned}, \quad (1.38)$$

which indicates that all non-zero eigenvalues of \mathbf{B} satisfy

$$\lambda_i(\mathbf{B}) \in \left\{ \lambda \left(\mathbf{U}^T \mathbf{U} - \frac{1}{\gamma} \mathbf{I} \right) \right\} = \left\{ -\frac{1}{\gamma}, 1 - \frac{1}{\gamma} \right\}. \quad (1.39)$$

Due to the redundancy, there exists $\mathbf{a} \neq \mathbf{0}$ such that $\Psi^* \mathbf{a} = \mathbf{0}$. Thus there are zero eigenvalues of \mathbf{B} . Together, we have

$$\begin{aligned} \lambda_i(\mathbf{B}) &= 0 \quad \text{for some choices of } i \\ \& \lambda_i(\mathbf{B}) \in \left\{ -\frac{1}{\gamma}, 1 - \frac{1}{\gamma} \right\} \quad \text{for other choices of } i \end{aligned}. \quad (1.40)$$

Equation (1.40) indicates that

$$L(\gamma) = \max_i \left\{ \lambda_i(\mathbf{B}) + \frac{1}{\gamma} \right\} = \frac{1}{\gamma}, \quad 0 \leq \gamma \leq 1 \quad (1.41)$$

$$L(\gamma) = \max_i \left\{ \lambda_i(\mathbf{B}) + \frac{1}{\gamma} \right\} \leq 1, \quad \gamma \geq 1$$

Done proof of (1.35).

The relation (1.35) or (1.41) means that, when $0 < \gamma \leq 1$, one has $L(\gamma) = 1/\gamma$. This together with [23] implies that pFISTA will converge with speed described in (1.28).

Done proof of **Theorem 1**.

C. Connections with Balanced Sparse Model

As is shown in last section, pFISTA converges to an approximate model (1.27) instead of the exact analysis model (1.3) or (1.16). The model (1.27) is not new in general image restoration and it was called the balanced sparse model that balances solutions between synthesis and analysis sparse models [27, 32, 33]. Shen *et al.* [27] proposed an accelerated proximal gradient algorithm (APG) to solve balanced sparse models in common image restoration tasks, including deblurring, denosing and component decomposition, but not CS-MRI problems. Although from different perspectives, it turns out that pFISTA coincides with APG when the linear operator is chosen as undersampling Fourier operator. However, pFISTA is not a trivial extension for following reasons:

1) Although tight frames are shown to improve the image quality significantly in CS-MRI, but how to solve tight frames-based MRI image reconstruction fast and with minimal free parameters is still unknown. The proposed pFISTA only

introduces one parameter, the step size, and experiments show that reconstruction errors are insensitive to this parameter (See Section III).

2) The APG algorithm is formulated and implemented in frame coefficients domain, and it needs to store copies of all redundant frame coefficients. Our pFISTA works in image domain, and there is no need to store any tight frame coefficients with a careful coding. Therefore, the pFISTA can significantly reduce memory consumption for highly redundant tight frames.

These two properties allow users in MRI to easily set algorithm parameters and utilize different tight frames for high quality image reconstruction from undersampled k-space data.

III. NUMERICAL EXPERIMENTS

In this section, we will verify the effectiveness and fast convergence speed of the proposed pFISTA for tight frames in CS-MRI by comparing it with FISTA [23] and SFISTA [25].

The brain MRI image of size 256×256 in Fig. 2 (a) is acquired from a healthy volunteer at a 3T Siemens Trio Tim MRI scanner using the T2-weighted turbo spin echo sequence (TR/TE = 6100/99 ms, FOV = 220×220 mm², slice thickness = 3 mm). The k-space undersampling is simulated by the mask in Fig. 2 (d) with 30% of k-space data is sampled. Note that in our application, the undersampling is only along the phase encoding dimension because the frequency encoding dimension is not time consuming and is unworthy of undersampling. The i.i.d. Gaussian noise with standard deviation $\sigma=0.02$ is added to the k-space and the corresponding noisy image is shown in Fig. 2 (b). We did not report more results on other MR images since consistent phenomenon are observed.

All numerical experiments are conducted on a Dell PC running Windows 7 operating system with Intel Core i7 2600 CPU. For numeric index we adopt the relative ℓ_2 norm error (RLNE) defined as

$$\text{RLNE} := \frac{\|\hat{\mathbf{x}} - \mathbf{x}\|_2}{\|\mathbf{x}\|_2}, \quad (1.42)$$

where \mathbf{x} is the ground truth image and $\hat{\mathbf{x}}$ is the reconstructed image. This criteria is widely used in MR image reconstructions [34-36].

Free parameters of algorithms are step size γ_F for FISTA, step size γ_S and smooth approximate parameter μ for SFISTA, and step size γ_p for pFISTA. $\gamma_F=1$ is set for fast convergence [23]. $\gamma_S=1/(1+1/\mu)$ is set and series of μ are tried according to [25]. $\gamma_p=1$ is set for both promising reconstruction performance and fast speed. All regularization parameters, λ_F of FISTA, λ_S of SFISTA and λ_p of pFISTA are set to achieve the lowest reconstruction errors for each method.

A. Main Result

The shift-invariant discrete wavelet transform (SIDWT)

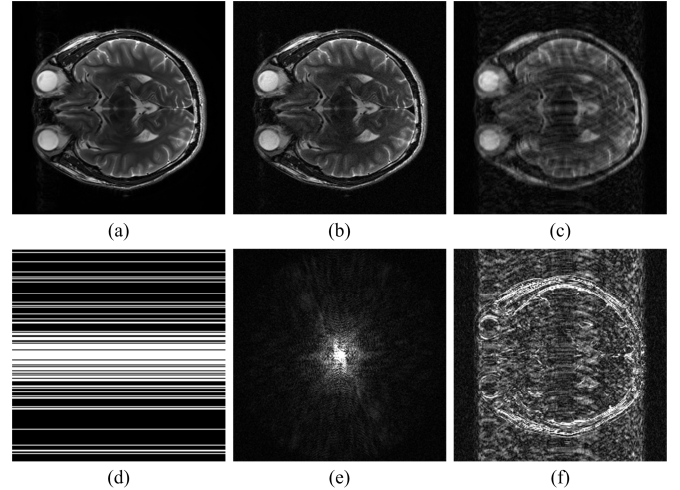


Fig. 2. Experimental dataset. (a) is the ground truth image. (b) is the noisy image. (c) is the zero-filling reconstruction. (d) is the sampling mask with horizontal is frequency encoding direction and vertical is phase encoding direction. (e) is the k-space of (b). (f) is the 5 times scaled difference image of (c) to (a).

implemented in Rice Wavelet Toolbox [37] is adopted as the tight frame for simulations in this section. We choose SIDWT as the typical tight frame since it is widely used to sparsify MR images and its redundant form can improve the reconstruction significantly over the orthogonal form [9]. The regularization parameters are $\lambda_F = \lambda_S = \lambda_p = 0.01$ in this case.

As shown in Fig. 3, the reconstructed image of FISTA exhibits obvious artifacts which are suppressed much better using SFISTA and pFISTA. The FISTA reaches to a higher reconstruction error while the latter two produce close errors. The original FISTA solves the synthesis sparse models, which usually produced sub-optimal results compared with analysis and balanced sparse models. This observation is consistent with other researchers [6, 10, 14, 15, 32].

The main difference between SFISTA and pFISTA is the convergence. SFISTA is sensitive to the smooth approximate parameter μ as shown in Fig. 4 (a). A larger μ leads to a faster convergence while reaching a higher RLNE error. pFISTA converges much faster than SFISTA but achieves comparable and also the lowest reconstruction errors of SFISTA.

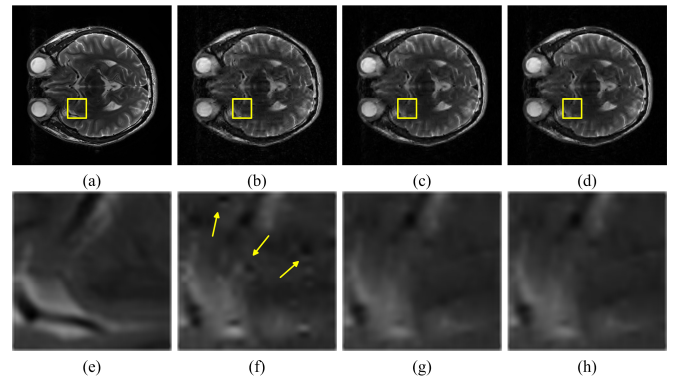


Fig. 3. Reconstructed images of FISTA, SFISTA and pFISTA for SIDWT. (a) is the ground truth image. (b)-(d) are reconstructed images of FISTA, SFISTA with $\mu=0.01$ and pFISTA and the RLNE errors are 0.207, 0.190 and 0.192 respectively. (e)-(h) are zoom-in images of the regions described in (a)-(d).

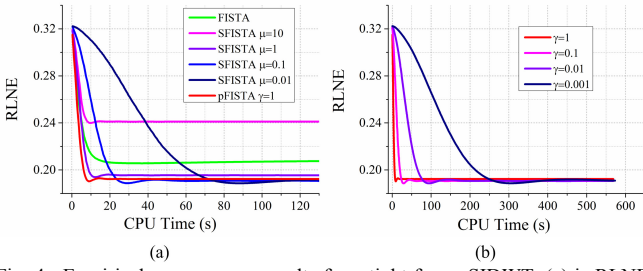


Fig. 4. Empirical convergence results for a tight frame SIDWT. (a) is RLNE errors of FISTA, SFISTA with different values of μ and pFISTA. (b) is RLNE errors of pFISTA with different values of γ .

B. Discussions

1) Sensitivity of pFISTA to the Step Size

As shown in the section of ‘convergence analysis’, the step size γ_p appears in the model (1.27) that pFISTA converges to. In this section, we will investigate how the step size can affect the convergence and reconstruction. Fig. 4 (b) shows that with a smaller γ_p , the convergence speed is slower while the final RLNE is almost not affected by γ_p . Therefore, the reconstruction error of pFISTA is insensitive to the step size parameter. This is why we recommend setting the $\gamma_p = 1$ for common use in tight frames based CS-MRI.

2) Experiments on Other Tight Frames

Different tight frames may affect convergence speed and reconstruction errors. Thus, it is worthy to discuss some other tight frames. In this section, we conduct experiments on another two tight frames that were used in CS-MRI: contourlets [38, 39] and patch based directional wavelets (PBDW) [35]. Both of them explore the geometric information to sparsely represent MR images thus improve edge reconstruction [35, 38, 39]. The regularization parameters for contourlet and PBDW are $\lambda_F = \lambda_S = \lambda_p = 0.01$ and $\lambda_F = \lambda_S = \lambda_p = 0.001$, respectively.

The same phenomenon are observed for two tight frames: 1) RLNE errors of SFISTA and pFISTA are lower than FISTA; 2) The RLNE error of SFISTA is sensitive to the smooth approximate parameter μ while the proposed pFISTA is stable to the step size parameter γ ; 3) the convergence speed of pFISTA are comparable or even faster than SFISTA.

3) Experiment on a Frame

In order to demonstrate the effectiveness of pFISTA for frames, we conduct another experiment using a frame proposed in [36] by one of the authors. This frame is called a patch-based non-local operator (PANO) [36] or BM3D frames [40] that is devised to utilize the self-similarity of MR images and optical images, respectively. Similar patches are grouped and sparsified with wavelets, PANO is a frame such that [36, 40]

$$\Psi^* \Psi = \Lambda, \quad (1.43)$$

where Λ is a diagonal matrix with diagonal elements represent the overlap factors of corresponding pixels thus are integers normally ranging from several to hundreds.

According to (1.8), the canonical dual frame of PANO is

$\Phi = \Lambda^{-1} \Psi^*$. In this case, setting the step size of pFISTA is

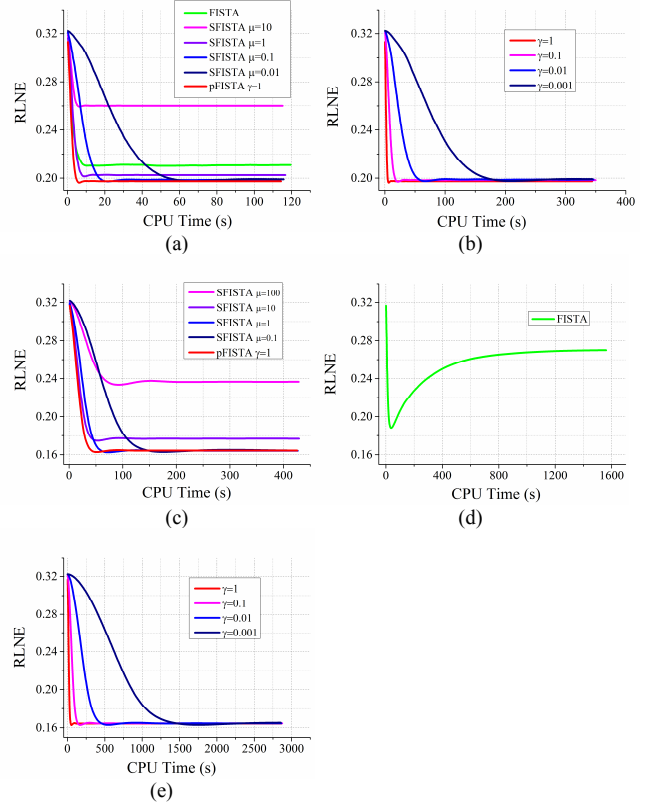


Fig. 5. Empirical convergence for contourlets and PBDW. (a) is RLNE errors of FISTA, SFISTA and pFISTA for contourlets. (b) is RLNE errors of pFISTA with different values of γ for contourlets. (c) is RLNE errors of SFISTA and pFISTA for PBDW. (d) is RLNE errors of FISTA for PBDW. (e) is RLNE errors of pFISTA with different values of γ for PBDW.

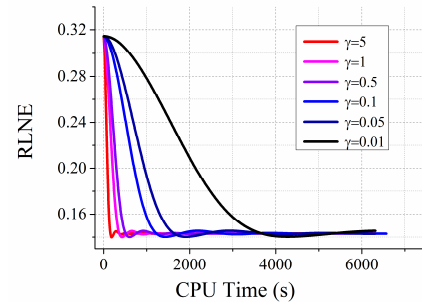


Fig. 6. Effect of the step size γ on reconstruction errors when a frame PANO is used in pFISTA.

relatively tricky. Fig. 6 shows that the reconstruction error of pFISTA is insensitive to the step size parameter γ , which is consistent to observations on tight frames.

IV. CONCLUSION

We propose a simple and fast algorithm, pFISTA, for tight frames in compressed sensing magnetic resonance imaging and prove its convergence. The proposed pFISTA converges faster or comparable to the state-of-the-art smoothing FISTA. One main advantage of pFISTA is that reconstructed errors are insensitive to the step size parameter, thus allowing widely

usage for different tight frames in magnetic resonance image reconstructions. One future work is to analyze the convergence of pFISTA for general frames.

APPENDIX

Proof of the equivalence between (1.16) and (1.3)

Denoting that $G(\mathbf{x}) = \lambda \|\Psi\mathbf{x}\|_1 + 1/2 \|\mathbf{y} - \mathbf{U}\mathbf{F}\mathbf{x}\|_2^2$, then one has

$$\begin{aligned} & \min_{\mathbf{a} \in \text{Range}(\Psi)} \lambda \|\mathbf{a}\|_1 + \frac{1}{2} \|\mathbf{y} - \mathbf{U}\mathbf{F}\Phi\mathbf{a}\|_2^2 \\ \stackrel{(a)}{=} & \min_{\mathbf{a} \in \text{Range}(\Psi)} \lambda \|\Psi\Phi\mathbf{a}\|_1 + \frac{1}{2} \|\mathbf{y} - \mathbf{U}\mathbf{F}\Phi\mathbf{a}\|_2^2 \\ \stackrel{(b)}{=} & \min_{\mathbf{a} \in \text{Range}(\Psi)} G(\Phi\mathbf{a}) \\ \stackrel{(c)}{=} & \min_{\mathbf{x} \in \Omega} G(\mathbf{x}) \end{aligned} \quad (1.44)$$

with $\Omega = \{\Phi\mathbf{a} \mid \mathbf{a} \in \text{Range}(\Psi)\}$ where (a) from the property (1.11) for $\mathbf{a} \in \text{Range}(\Psi)$, (b) and (c) are straightforward based on the definition of $G(\cdot)$ and Ω . Next, we show that $\Omega = \mathbb{C}^N$. On one hand, we have

$$\mathbf{x} \in \mathbb{C}^N \stackrel{\Phi\Psi\mathbf{x}=\mathbf{x}}{\Rightarrow} \mathbf{x} \in \Omega \text{ with } \mathbf{a} = \Psi\mathbf{x}. \quad (1.45)$$

On the other hand, we have

$$\begin{aligned} & \mathbf{x} \in \Omega \\ \Rightarrow & \mathbf{x} = \Phi\mathbf{a} \text{ for some } \mathbf{a} \in \text{Range}(\Psi) \\ \Rightarrow & \mathbf{x} = \Phi\mathbf{a} \text{ with } \mathbf{a} = \Psi\tilde{\mathbf{x}} \text{ for some } \tilde{\mathbf{x}} \in \mathbb{C}^N \\ \Rightarrow & \mathbf{x} = \Phi\Psi\tilde{\mathbf{x}} = \tilde{\mathbf{x}} \text{ for some } \tilde{\mathbf{x}} \in \mathbb{C}^N \\ \Rightarrow & \mathbf{x} \in \mathbb{C}^N \end{aligned} \quad (1.46)$$

(1.45) and (1.46) together leads to $\Omega = \mathbb{C}^N$. This together with (1.44) leads to

$$\begin{aligned} & \min_{\mathbf{a} \in \text{Range}(\Psi)} \lambda \|\mathbf{a}\|_1 + \frac{1}{2} \|\mathbf{y} - \mathbf{U}\mathbf{F}\Phi\mathbf{a}\|_2^2 \\ = & \min_{\mathbf{x}} \lambda \|\Psi\mathbf{x}\|_1 + \frac{1}{2} \|\mathbf{y} - \mathbf{U}\mathbf{F}\mathbf{x}\|_2^2 \end{aligned} \quad (1.47)$$

If \mathbf{a}^* is a solution of (1.16) and \mathbf{x}^* is a solution of (1.3), then one has

$$G(\Phi\mathbf{a}^*) \stackrel{(d)}{=} G(\mathbf{x}^*) \stackrel{(e)}{=} G(\Phi\Psi\mathbf{x}^*) \quad (1.48)$$

where (d) from the second equation in (1.44) and (1.47), (e) from (1.9). Therefore, $\Phi\mathbf{a}^*$ is also a solution of the analysis model (1.3) and $\Psi\mathbf{x}^*$ is also a solution of the synthesis-like model (1.16).

Done proof.

REFERENCES

- [1] M. Lustig, D. Donoho, and J. M. Pauly, "Sparse MRI: The application of compressed sensing for rapid MR imaging," *Magnetic Resonance in Medicine*, vol. 58, pp. 1182-1195, 2007.
- [2] E. J. Candes, J. Romberg, and T. Tao, "Robust uncertainty principles: exact signal reconstruction from highly incomplete frequency information," *IEEE Transactions on Theory Information*, vol. 52, pp. 489-509, 2006.
- [3] D. L. Donoho, "Compressed sensing," *IEEE Transactions on Theory Information*, vol. 52, pp. 1289-1306, 2006.
- [4] S. Nam, M. E. Davies, M. Elad, and R. Gribonval, "The cosparse analysis model and algorithms," *Applied and Computational Harmonic Analysis*, vol. 34, pp. 30-56, 2013.
- [5] E. J. Candes, Y. C. Eldar, D. Needell, and P. Randall, "Compressed sensing with coherent and redundant dictionaries," *Applied and Computational Harmonic Analysis*, vol. 31, pp. 59-73, 2011.
- [6] M. Elad, P. Milanfar, and R. Rubinstein, "Analysis versus synthesis in signal priors," *Inverse problems*, vol. 23, p. 947, 2007.
- [7] J. L. Starck, J. Fadili, and F. Murtagh, "The undecimated wavelet decomposition and its reconstruction," *IEEE Transactions on Image Processing*, vol. 16, pp. 297-309, 2007.
- [8] R. R. Coifman and D. L. Donoho, "Translation-invariant de-noising," in *Wavelets and Statistics*, vol. 103, A. Antoniadis and G. Oppenheim, Eds., ed: Springer New York, 1995, pp. 125-150.
- [9] C. A. Baker, K. King, L. Dong, and Y. Leslie, "Translational-invariant dictionaries for compressed sensing in magnetic resonance imaging," *Proceedings of 2011 IEEE International Symposium on Biomedical Imaging: From Nano to Macro-ISBI'11*, pp. 1602-1605, 2011.
- [10] Y. Liu, J.-F. Cai, Z. Zhan, D. Guo, J. Ye, Z. Chen, and X. Qu, "Balanced sparse model for tight frames in compressed sensing magnetic resonance imaging," *PLoS One*, vol. 10, e0119584, 2015.
- [11] M. Guerquin-Kern, M. Haberlin, K. P. Pruessmann, and M. Unser, "A fast wavelet-based reconstruction method for magnetic resonance imaging," *IEEE Transactions on Medical Imaging*, vol. 30, pp. 1649-1660, 2011.
- [12] S. Ravishanker and Y. Bresler, "MR image reconstruction from highly undersampled k-space data by dictionary learning," *IEEE Transactions on Medical Imaging*, vol. 30, pp. 1028-1041, 2011.
- [13] Q. Liu, S. Wang, Y. Leslie, X. Peng, Y. Zhu, and D. Liang, "Adaptive dictionary learning in sparse gradient domain for image recovery," *IEEE Transactions on Image Processing*, vol. 22, pp. 4652-4663, 2013.
- [14] I. W. Selesnick and M. A. T. Figueiredo, "Signal restoration with overcomplete wavelet transforms: comparison of analysis and synthesis priors," *Proceedings of SPIE*, vol. 7446, August 2-4, 2009.
- [15] A. Majumdar and R. K. Ward, "On the choice of compressed sensing priors and sparsifying transforms for MR image reconstruction: An experimental study," *Signal Processing: Image Communication*, vol. 27, pp. 1035-1048, 2012.
- [16] J.-F. Cai, B. Dong, S. Osher, and Z. Shen, "Image restoration: Total variation, wavelet frames, and beyond," *Journal of the American Mathematical Society*, vol. 25, pp. 1033-1089, 2012.
- [17] I. Daubechies, M. Defrise, and C. De Mol, "An iterative thresholding algorithm for linear inverse problems with a sparsity constraint," *Communications on Pure and Applied Mathematics*, vol. 57, pp. 1413-1457, 2004.
- [18] P. Combettes and V. Wajs, "Signal recovery by proximal forward-backward splitting," *Multiscale Modeling & Simulation*, vol. 4, pp. 1168-1200, 2005.
- [19] N. Parikh and S. Boyd, "Proximal algorithms," *Foundations and Trends in Optimization*, vol. 1, pp. 123-231, 2013.
- [20] M. Zibulevsky and M. Elad, "L1-L2 optimization in signal and image processing," *IEEE Signal Processing Magazine*, vol. 27, pp. 76-88, 2010.
- [21] M. A. T. Figueiredo, R. D. Nowak, and S. J. Wright, "Gradient projection for sparse reconstruction: Application to compressed sensing and other inverse problems," *IEEE Journal of Selected Topics in Signal Processing*, vol. 1, pp. 586-597, 2007.
- [22] J. Huang, S. Zhang, and D. Metaxas, "Efficient MR image reconstruction for compressed MR imaging," *Medical Image Analysis*, vol. 15, pp. 670-679, 2011.
- [23] A. Beck and M. Teboulle, "A fast iterative shrinkage-thresholding algorithm for linear inverse problems," *SIAM Journal on Imaging Sciences*, vol. 2, pp. 183-202, 2009.
- [24] P. Combettes and J.-C. Pesquet, "Proximal splitting methods in signal processing," *Fixed-Point Algorithms for Inverse Problems in Science and Engineering*, vol. 49, pp. 185-212, 2011.
- [25] Z. Tan, Y. C. Eldar, A. Beck, and A. Nehorai, "Smoothing and decomposition for analysis sparse recovery," *IEEE Transactions on Signal Processing*, vol. 62, pp. 1762-1774, 2014.

- [26] M. Vetterli, J. Kovačević, and V. K. Goyal, *Foundations of Signal Processing*, 2013.
- [27] Z. Shen, K.-C. Toh, and S. Yun, "An accelerated proximal gradient algorithm for frame-based image restoration via the balanced approach," *SIAM Journal on Imaging Sciences*, vol. 4, pp. 573-596, 2011.
- [28] J.-F. Cai, R. H. Chan, and Z. W. Shen, "A framelet-based image inpainting algorithm," *Applied and Computational Harmonic Analysis*, vol. 24, pp. 131-149, 2008.
- [29] D. S. Weller, S. Ramani, and J. A. Fessler, "Augmented Lagrangian with variable splitting for faster non-Cartesian L1-SPIRiT MR image reconstruction," *IEEE Transactions on Medical Imaging*, vol. 33, pp. 351-361, 2014.
- [30] X. Ye, Y. Chen, W. Lin, and F. Huang, "Fast MR image reconstruction for partially parallel imaging with arbitrary k-space trajectories," *IEEE Transactions on Medical Imaging*, vol. 30, pp. 575-585, 2011.
- [31] B. Zhao, W. Lu, T. K. Hitchens, F. Lam, C. Ho, and Z.-P. Liang, "Accelerated MR parameter mapping with low-rank and sparsity constraints," *Magnetic Resonance in Medicine*, DOI: 10.1002/mrm.25421, 2014.
- [32] J.-F. Cai, S. Osher, and Z. Shen, "Split Bregman methods and frame based image restoration," *Multiscale Modeling & Simulation*, vol. 8, pp. 337-369, 2009.
- [33] J.-F. Cai, H. Ji, Z. Shen, and G.-B. Ye, "Data-driven tight frame construction and image denoising," *Applied and Computational Harmonic Analysis*, vol. 37, pp. 89-105, 2014.
- [34] B. Ning, X. Qu, D. Guo, C. Hu, and Z. Chen, "Magnetic resonance image reconstruction using trained geometric directions in 2D redundant wavelets domain and non-convex optimization," *Magnetic Resonance Imaging*, vol. 31, pp. 1611-1622, 2013.
- [35] X. Qu, D. Guo, B. Ning, Y. Hou, Y. Lin, S. Cai, and Z. Chen., "Undersampled MRI reconstruction with patch-based directional wavelets," *Magnetic Resonance Imaging*, vol. 30, pp. 964-977, 2012.
- [36] X. Qu, Y. Hou, F. Lam, D. Guo, J. Zhong, and Z. Chen, "Magnetic resonance image reconstruction from undersampled measurements using a patch-based nonlocal operator," *Medical Image Analysis*, vol. 18, pp. 843-856, 2014.
- [37] R. Baraniuk, H. Choi, R. Neelamani, V. Ribeiro, J. Romberg, H. Guo, *et al.* (2009). *Rice wavelet toolbox*. Available: <http://dsp.rice.edu/software/rice-wavelet-toolbox>
- [38] M. N. Do and M. Vetterli, "The contourlet transform: an efficient directional multiresolution image representation," *IEEE Transactions on Image Processing*, vol. 14, pp. 2091-2106, 2005.
- [39] X. Qu, W. Zhang, D. Guo, C. Cai, S. Cai, and Z. Chen, "Iterative thresholding compressed sensing MRI based on contourlet transform," *Inverse Problems in Science and Engineering*, vol. 18, pp. 737-758, 2010.
- [40] A. Danielyan, V. Katkovnik, and K. Egiazarian, "BM3D frames and variational image deblurring," *IEEE Transactions on Image Processing*, vol. 21, pp. 1715-1728, 2012.